ELSEVIER

Journal of Structural Geology 30 (2008) 394–405

JOURNAL OF STRUCTURAL GEOLOGY

www.elsevier.com/locate/jsg

Displacement loss on growth faults due to sediment compaction

Susanna K. Taylor [a], Andrew Nicol [a,b], John J. Walsh [a,*]

[a] *Fault Analysis Group, UCD School of Geological Sciences, University College Dublin, Belfield, Dublin 4, Ireland*
[b] *GNS Science, Lower Hutt, New Zealand*

Received 22 December 2006; received in revised form 30 October 2007; accepted 13 November 2007
Available online 19 November 2007

Abstract

Compaction models of normal growth faults, combined with displacement data from a natural growth fault (Cape Egmont Fault, New Zealand), are used to quantify the loss of displacement arising from compaction, in circumstances where growth faults are blanketed and buried by compacting sediment in both footwall and hangingwall. Comparison of imposed tectonic displacements with the preserved displacements indicates that although the thicknesses of sand/shale sequences may decrease by up to c. 55% due to compaction, associated losses in displacement on growth faults are typically <20% because they displace partially compacted sediments. The importance of displacement loss generally increases with increases in the depth range over which fault displacements migrate along the compaction curves and in the percentage shale of the faulted sequence. Displacement loss due to compaction is relatively small (<c. 15%) for sand or mixed sand-shale sequences with growth indices greater than c. 0.1 (equivalent to the ratio of the fault throw rate and footwall sedimentation rate), and in these strata decompaction is not required to decipher first-order displacements and fault-growth histories. Decompaction of displacements is of most benefit in circumstances where growth sequences have a high shale content (>70%) and post-faulting burial is large (i.e. km-scale).

Keywords: Normal growth faults; Compaction; Displacement

1. Introduction

Displacement on normal faults commonly provides the most obvious and quantifiable measure of extension in sedimentary rocks. Many recent studies of the kinematics of normal faults have used sequence growth to characterise the displacement history of synsedimentary faults (e.g. Roux, 1979; Petersen et al., 1992; Childs et al., 1993, 1995, 2003; McLeod et al., 2000; Meyer et al., 2002; Walsh et al., 2002). In circumstances where fault footwall sedimentation rates outstrip displacement rates at the free surface, sequence growth from fault footwall to hangingwall reflects displacement accumulation that is accompanied by progressive upward decreases in displacement on younger syn-faulting horizons (Fig. 1). These displacement and thickness changes provide a basis for reconstructing the kinematic history of faulting. Displacement backstripping is one means of reconstructing the history of displacement accumulation and involves the sequential removal of displacements on successively older syn-faulting horizons from displacements on the horizon at the base of the syn-faulting sequence (Childs et al., 1993, 2003; Clausen et al., 1994). A basic assumption of this, and other restoration methods, is that incremental displacements (i.e. short-term displacements) within the syn-faulting sequence are constant on individual cross-sections. In detail this assumption must breakdown because sediment compaction will lead to subsequent decreases in those incremental displacements by amounts which will decline with increasing depth and pre-displacement sediment compaction.

Compaction arising from sediment accumulation has been extensively studied (e.g. Hedberg, 1936; Weller, 1959; Perrier and Quiblier, 1974; Sclater and Christie, 1980; Baldwin and Butler, 1985; Lundegard, 1992), however, the magnitude of changes in fault displacements arising from compaction is poorly understood. Determining the influence of compaction on fault displacements has become increasingly important in

* Corresponding author. Tel.: +353 1 716 2605; fax: +353 1 716 2607.
E-mail address: john@fag.ucd.ie (J.J. Walsh).

0191-8141/$ - see front matter © 2007 Elsevier Ltd. All rights reserved.
doi:10.1016/j.jsg.2007.11.006

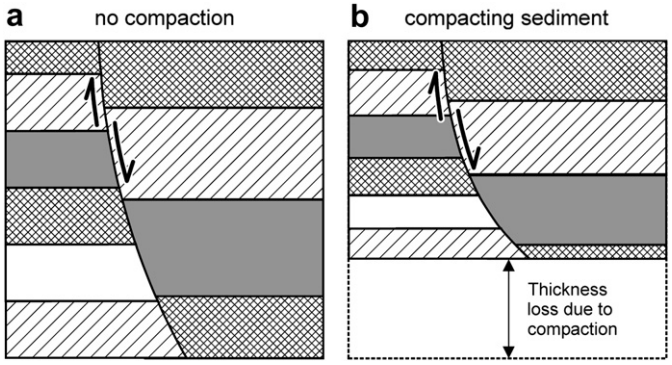

Fig. 1. Schematic diagrams illustrating the effect of compaction on layer thicknesses, fault displacements and fault dips.

recent years with the widespread availability of seismic reflection profiles and an increase in the use of displacements to draw conclusions about the systematics of fault displacement patterns, fault-size distributions, fault growth and regional strain patterns (e.g. Watterson, 1986; Barnett et al, 1987; Walsh et al., 1991; Schlische et al., 1996; McLeod et al., 2000; Meyer et al., 2002). The purpose of this article is to examine the extent to which conclusions on fault systematics based on their displacements would be modified by incorporating the effects of compaction. We use sediment compaction models of growth faults in tandem with displacement data from a natural fault (Cape Egmont Fault, New Zealand) to quantify the displacement loss due to compaction by comparing initial (tectonic) and final (tectonic and compaction) displacements. This article only considers those faults which are continuously buried, as these faults are most amenable to the measurement and analysis of displacements. We do not model faults with footwall uplift and hangingwall subsidence that locally produce erosion and underfilled basins (e.g. Gibson et al., 1989), respectively, and nor do we consider circumstances in which the compaction properties of the footwall and hangingwall sequences are different. Our study shows that despite the apparent importance of compaction (Fig. 1), its effects on fault displacements are often relatively subdued and can, for some purposes, be neglected. Future studies of fault displacements may, however, benefit from decompaction where shale content is high (e.g. >70%) and post-faulting burial is important.

2. Methods for estimating compaction-induced displacement changes

Faults enclosed within sediments and sedimentary rocks generally experience compaction due to a progressive increase of overburden load during burial. Compaction results in a decrease of thickness of sedimentary units associated with progressive expulsion of pore fluid and reduction of pore space, processes which ultimately result in porosity loss (Perrier and Quiblier, 1974; Sclater and Christie, 1980; Lundegard, 1992). The amount of compaction is mainly dependent on the sediment type and the depth of burial. In this article we show that although the compaction of strata can exceed 50%, the resulting decrease in fault displacement is typically much less (e.g. <20%). The reason for this is that the magnitude of displacement decrease due to compaction depends on the relative timing of compaction and faulting, rather than simply reflecting the absolute compaction of sediment enclosing the fault. Displacements accumulated when sediments are close to the free surface, and are therefore poorly compacted, will be poorly preserved compared to those which are accumulated when the same sediments are at greater burial depths and are more compacted. The preservation of original (i.e. uncompacted) displacements is therefore optimised where displacement accumulates within sedimentary rocks that have already experienced significant compaction; this factor accounts for the more subdued impact of compaction on fault displacements than sediment thicknesses.

Compaction analysis is conducted in this article using models for sequences with varying proportions of sand and shale, differing ranges of ratios of fault displacement to footwall sedimentation rates, and for varying proportions of pre-, syn- and post-faulting sedimentation (Fig. 2). Our modelling focuses on syndepositional normal faults with up to km-scale displacements which are continuously blanketed by sediments (i.e. fault displacement rates exceed sedimentation rates) and are encased in compactable sediments. Thickness changes of sedimentary layers due to compaction, and associated decreases in fault displacement and layer thickness, were estimated using the porosity–depth functions of Sclater and Christie (1980; see their table A1a and our Fig. 3a). The theory and equations used to calculate sediment compaction and the resulting changes in porosity, layer thickness and displacement with increasing depth are presented in Appendix A.

Our modelling of the impact of compaction on the observed fault displacements involves the imposition of original tectonic displacements and computation of the magnitude of compaction-induced decreases in displacement for different sediment types, sedimentation rates (i.e. rates of burial) and fault displacement histories. To maintain a relatively manageable number of modelling parameters we have excluded certain parameters or issues from our modelling, for a variety of reasons. We assume that both pre-faulting and syn-faulting sequences compact in the same manner (with the same porosity–depth functions) and do not, for example, investigate the relatively common situation in which the pre-faulting footwall sequence, sometimes representing the ‘‘basement’’, is less compactable than the hangingwall sequence. In that respect, our models investigate circumstances in which fault displacements are most likely to be diminished by compaction because pre-compacted rocks, such as basement, will preserve displacements better. The exclusion of pre-compacted footwall sequences also simplifies our models insofar as we do not then have to confront the poorly studied issue of compaction-driven fault displacements, in which displacement on a fault may be driven by differential compaction of the hangingwall and footwall sequences. Our models also simply consider the loss of displacement on a notional vertical fault, rather than introducing fault dip as a parameter, for three

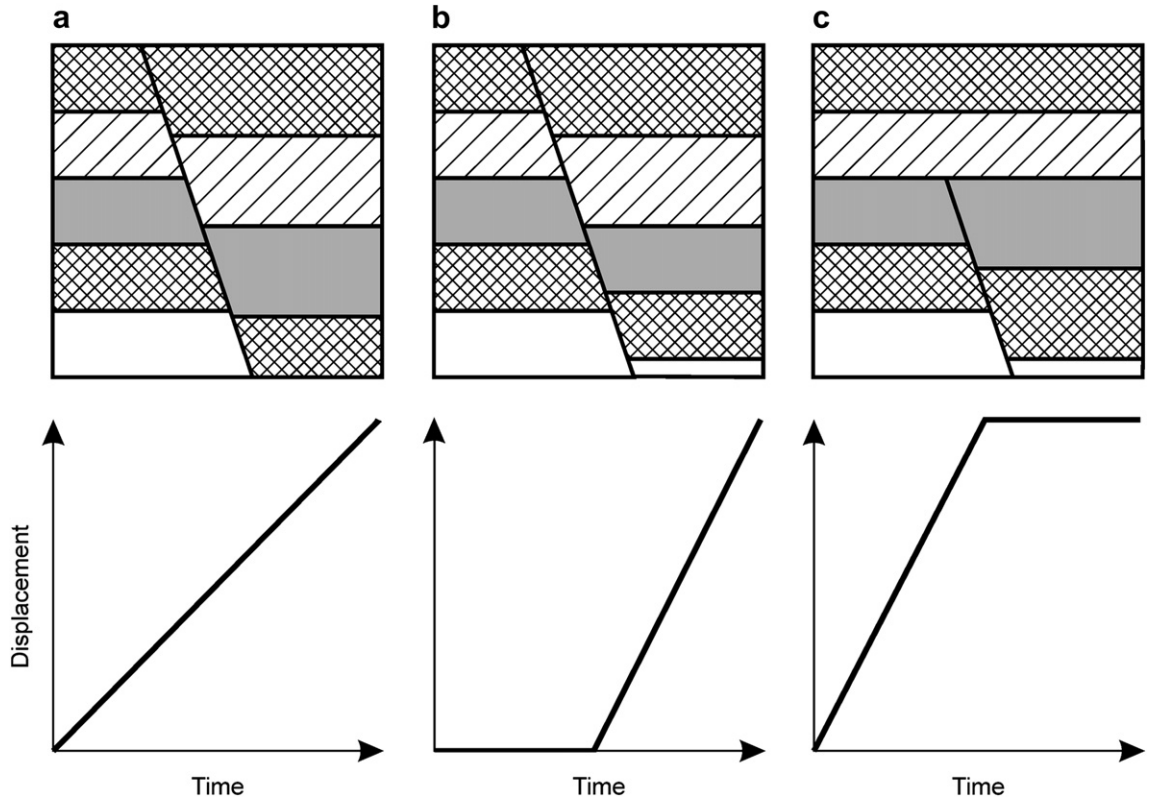

Fig. 2. Schematic diagrams illustrating the Constant (a), Late (b) and Early (c) fault displacement accumulation models examined and their associated displacement-time curves (see text for details).

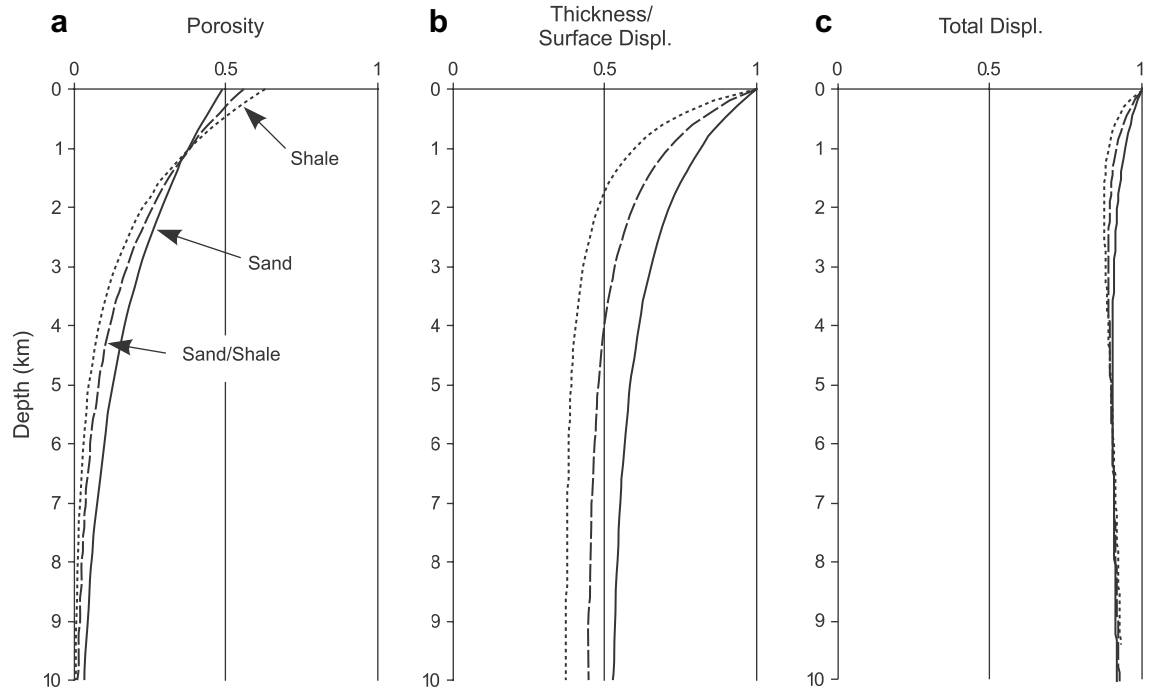

Fig. 3. Curves of porosity, thickness and displacement against depth for sand (solid line), sandy-shale (dashed line) and shale (dotted line) sequences. (a) Porosity–depth functions highlighting the exponential porosity decrease with depth, using values of surface porosity and compaction coefficient from Sclater and Christie (1980). Porosity values are given as a fraction of the rock volume. (b) The reduction in length (i.e. thickness) of a sediment column (i.e. sequence) caused by porosity loss. The curve is computed on the basis that the sequence thickness is so thin that the porosity at the base of the column is the same as the porosity at the top. (c) Fractional displacement curve, recording the fraction of post-compaction displacement preservation for a fault with a growth index of 1.

principal reasons. Firstly, vertical faults are most susceptible to displacement changes arising from compaction, because conventional compaction models generate a decrease in the vertical component of displacement (i.e. fault throw), without changing the horizontal component of displacement (i.e. fault heave). Secondly, in accordance with the majority of fault data, in which the horizontal location of horizon cutoffs are known less precisely than the vertical, the vertical component of displacement (i.e. the vertical separation between fault footwall and hangingwall horizon cutoffs) is the most robust measure of displacement. Finally, the inclusion of fault dip would require detailed consideration of compaction-related changes in fault dip with depth (e.g., Davison, 1987; Xiao and Suppe, 1989), an issue which will only diminish the impact of compaction on fault displacements and is beyond the scope of this article.

Our basic modelling configuration therefore highlights the maximum changes in displacement arising from compaction, by investigating the displacement, i.e. throw, changes associated with vertical faults. Fault growth is assumed to involve constant incremental displacements along the cross-sectional length of a fault, a reasonable base-line assumption for modelling of this type (see Childs et al., 1993, 2003), with sequence deposition defined by strata deposited across the fault as horizontal layers (Fig. 4; see below). Perhaps the most likely departure from constant incremental displacements would be an upward decrease in incremental displacements through the syn-faulting sequence, arising from associated rheological changes. Although the nature and degree of any such decrease has yet to be constrained, its presence would lead to better preservation of displacements because a higher proportion of displacement would accumulate at depths where associated sediments are better compacted. Our modelling approach therefore provides a better basis for highlighting the potential losses in displacement arising from compaction.

Models were produced for growth faults with three displacement histories: (1) constant displacement rates (i.e. Continuous faulting), (2) constant displacement rates preceded by a period of no faulting (i.e. Late faulting) and, (3) constant displacement rates followed by no faulting (i.e. Early faulting) (Fig. 2). In each of these fault displacement models compaction and the resulting decrease in displacements are calculated for sand, shale and mixed (50% sand and shale) sequences, and for ratios of displacement to footwall sediment thickness of 10, 1, 0.1 and 0.01 (Fig. 5). These ratios, which are referred to as growth indices, record the relative sedimentation rates on each side of the fault. Growth Index can be formally defined as the ratio of the difference in hangingwall and footwall thicknesses divided by the footwall thickness, and is the equivalent of the ratio of the throw rate to the footwall sedimentation rate. Modifications to growth indices can therefore arise due to changes in fault displacement rates, to variations in sedimentation rates or from a mixture of both: low growth indices require that fault displacement rates are low compared to sedimentation rates in the fault footwall. Following deposition, the growth index of a given layer will change as it is progressively buried and faulted, but this change is very small compared to the broad range of growth indices considered in our suite of models.

Each numerical model was constructed using three basic steps (Fig. 4; see Appendix A). (1) An initial horizontal horizon is faulted with the hangingwall displaced downwards by the throw (Fig. 4a). (2) A sediment layer is deposited over

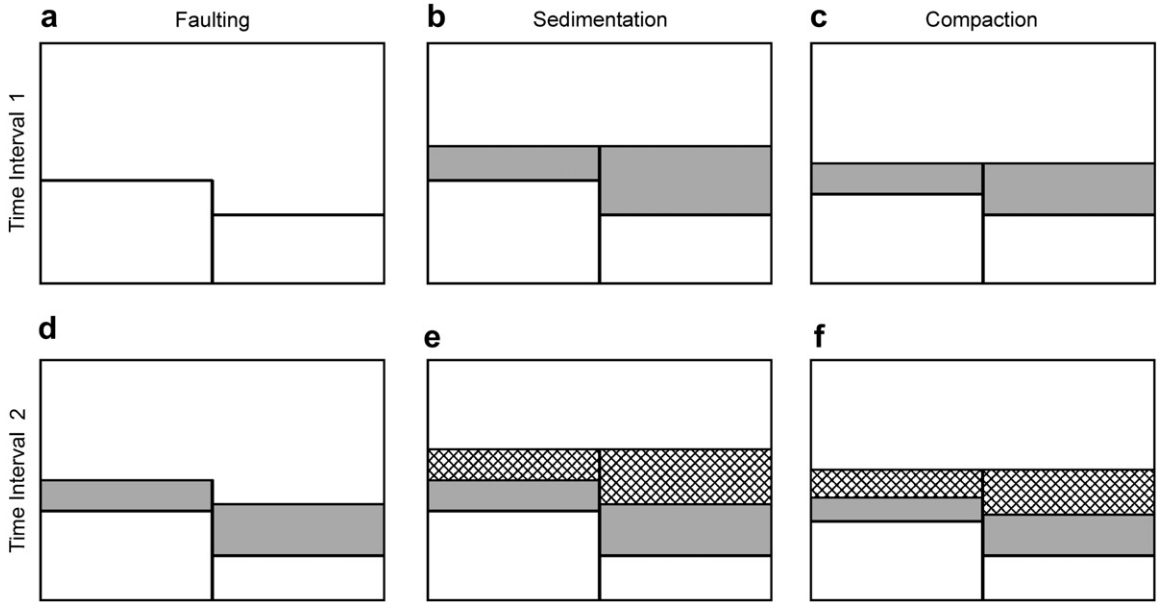

Fig. 4. Schematic representation of the three basic steps used in modelling of sediment compaction during fault growth (see text for details). (a) Step 1: A displacement increment is applied to fault cross-cutting an horizon. (b) Step 2: A sediment layer is deposited so that it extends horizontally over both hangingwall and footwall, burying the footwall by an amount equivalent to the subsidence rate (i.e. footwall sedimentation rate). (c) Step 3: The elevation of the hangingwall cutoff is readjusted (i.e. raised) accounting for the compaction associated with the deposition of layer in Step 2. (d–f) Steps 1–3 are repeated for a further increment of displacement and the addition of another layer of sediment.

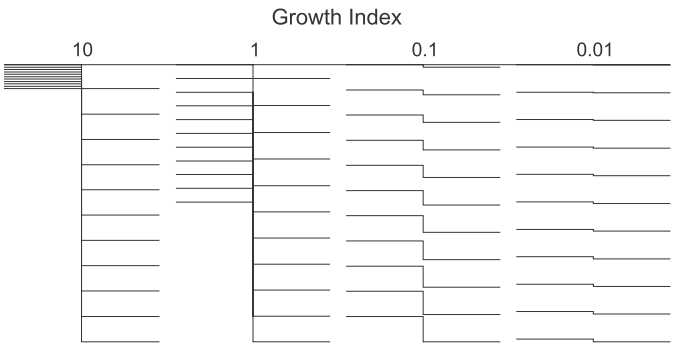

Fig. 5. Diagram showing the footwall–hangingwall relationships for faults with growth indices of 10, 1, 0.1 and 0.01. Each example shows the changing position of a given horizon as it accumulates increasing displacement and becomes progressively buried. Growth index is defined as the difference in hangingwall and footwall thicknesses divided by the footwall thickness, and is the equivalent of the ratio of the vertical displacement (i.e. throw) rate to the footwall sedimentation rate. Displacements or displacement changes on synsedimentary faults with growth indices greater than c. 10 or less than c. 0.01 will, in practical terms, be difficult to measure (see text for details).

both hangingwall and footwall to a constant vertical position, with the top of the layer horizontal and continuous across the fault (Fig. 4b). For the purposes of the modelling, the thickness of footwall sediment is equal to the subsidence across the model (i.e. variable water depths are not considered). (3) The depth of the hangingwall cutoff is readjusted (i.e. raised) to account for compaction arising from the addition of the layer deposited in (2). This compaction decreases the vertical distance (i.e. displacement) between the footwall and hangingwall cutoffs, leading to a decrease in the displacement accumulated in (1); the footwall depth is not altered because the footwall sequence is taken to be fully compacted. Steps 1–3 are repeated (e.g. Fig. 4d–f) and the footwall and hangingwall depths, and therefore associated displacements and sedimentation rates, are recorded for the faulted horizon at each step in the model (see Appendix A).

Changes in displacement arising from compaction highlighted by the modelling (Figs. 6 and 7) are later compared to the decrease in displacement generated by compaction of the syn-faulting sequence adjacent to the Cape Egmont Fault in the offshore Taranaki Basin, New Zealand (Fig. 8). The Cape Egmont Fault has displaced a sand/shale sequence (40% sand) by up to 2400 m since 3.7 Ma (Nicol et al., 2005). Pre-compaction displacements were derived for the Cape Egmont Fault by decompacting progressively older layers and at each stage recording the incremental uncompacted displacement before backstripping this displacement from underlying horizons. These data permit the generation of a displacement history curve (Fig. 9) equivalent to those presented in Fig. 7, which can then be directly compared with that derived from displacement backstripping without accounting for compaction.

3. Displacement changes; numerical modelling results

The effect of compaction on displacements for models with a range of rock types, growth indices and fault-timing scenarios are presented in Figs. 6 and 7. These plots indicate that compaction decreases the measured displacement relative to the applied uncompacted displacements by up to 30%, but with values which are typically $\leq$20%. To a first approximation, therefore, displacement history plots that do not incorporate decompaction provide a reasonable estimate of fault growth. As would be expected, displacement losses due to compaction increase with increasing percentage shale, because shale generally undergoes greater porosity loss than sand, and with increasing post-faulting burial.

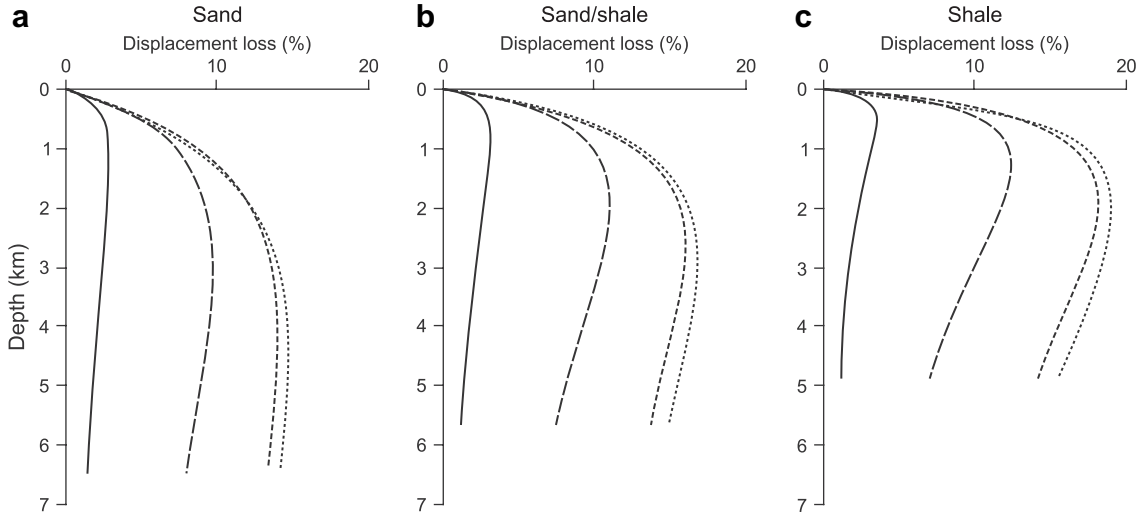

Fig. 6. Percentage loss in displacement, arising from compaction, relative to the original uncompacted (i.e. tectonic) displacement plotted against footwall depth. Results are shown for growth indices of 10 (solid), 1 (long dashes), 0.1 (short dashes) and 0.01 (dots), for faults contained within sand (a), shale (c) and mixed (sand/shale) (b) sequences. Grey polygons define growth indices and depths typical of natural faults (e.g. Childs et al., 2003): see text for details. Growth indices were modified by changing the fault displacement rate and maintaining constant footwall sedimentation rates. This approach generates faults with variations in growth indices which are equivalent to faults of different size (i.e. displacement, where displacement is the product of the footwall depth and growth index) populating a basin with a constant fault footwall sedimentation rate. Because the compaction-related displacement decreases are presented as a percentage of the original uncompacted displacement, the results are independent of how the faults with different growth indices were produced.

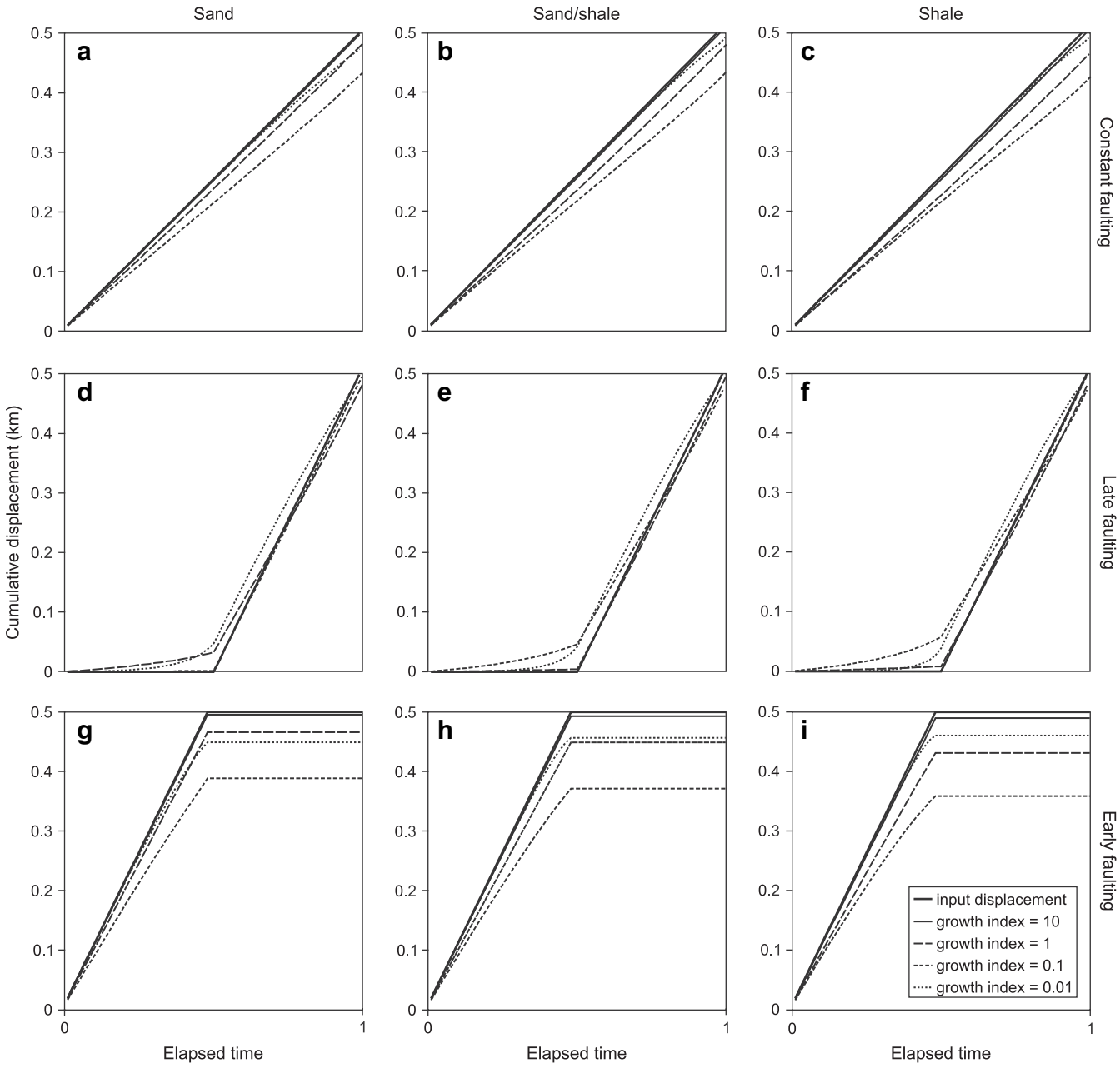

Fig. 7. Reconstructed fault displacement history showing the effect of different displacement histories and fault displacement to subsidence rates (i.e. growth index). Although the fault reaches a pre-compaction displacement of 500 m in each case, with displacement following different paths (heavy solid curves in each plot), the total displacement loss due to compaction is dependent on the sedimentation rate/burial history. See text and Fig. 2 for details.

Relations between percentage displacement loss arising from compaction and the depth of the footwall sequence are shown in Fig. 6 for sand (a), sand and shale (b) and shale (c) sequences with growth indices of 10, 1, 0.1 and 0.01. All of the curves in Fig. 6 show a similar form, with an initially rapid increase in percentage displacement loss in the upper kilometre, reaching a maximum loss at depths of c. 0.5–4 km, with losses decreasing below this point. These broad changes in the displacement loss reflect the exponential shape of the porosity–depth curves which require that most porosity loss is at shallow depths (c. 0.5–4 km) (Fig. 3a). For a given growth index and for the porosity–depth functions used, shale sequences display greater percentage loss of displacement in the upper 2–3 km than sands and lower percentage loss than sands below this depth (Sclater and Christie, 1980). For all lithologies the decrease in percentage displacement loss at depths $\geq$0.5–4 km arises because displacement that accumulates on layers below these depths undergoes less compaction than near-surface displacements which are subsequently buried. The importance of the relative timing of compaction and displacement accumulation is highlighted in Fig. 10, where displacement loss is illustrated for incremental displacements of 10 m that accrued on a fault at depths of 0, 1, 2, 3, 4 and 5 km and was subsequently buried to 5 km depth.

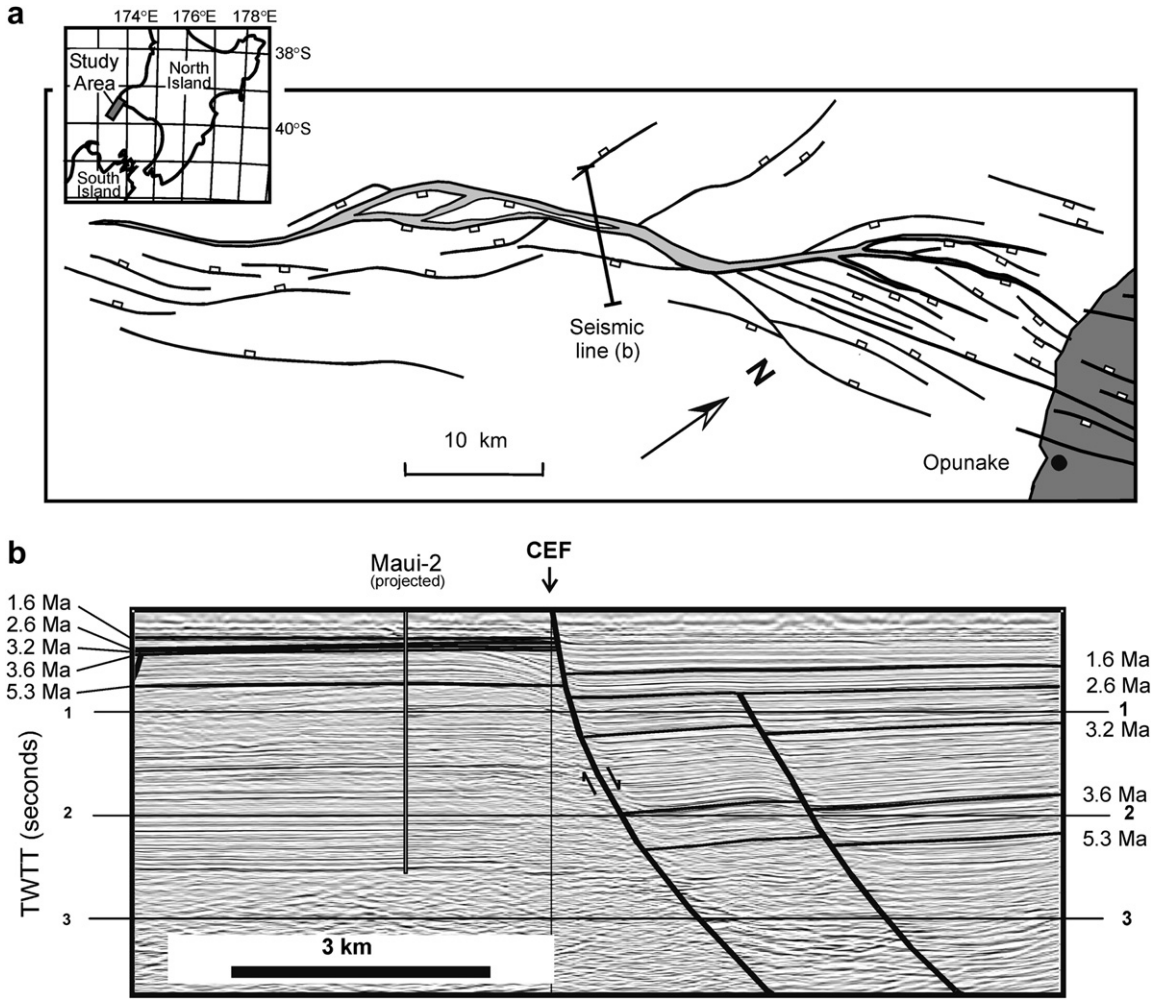

Fig. 8. Map on the base of the growth sequence and seismic section (86ma-46) of the Cape Egmont Fault, Taranaki Basin, New Zealand. This normal fault is imaged by 2D seismic reflection lines and has a maximum throw of about 2400 m that accrued over the last 3.7 Ma (Nicol et al., 2005). Measured displacements incorporated in our analysis (see Fig. 9) include fault throw and normal drag. The origin of a monoclinal flexure within the footwall of the pre-rift sequence is uncertain but its presence has no impact on our interpreted syn-rift fault displacements: examination of adjacent associated seismic lines, as well as a single seismic channel dataset, suggests that the monocline is probably a seismic artefact associated with much smaller amplitude normal drag (≤50 m) and/or minor footwall faults. Location of seismic line is shown on map.

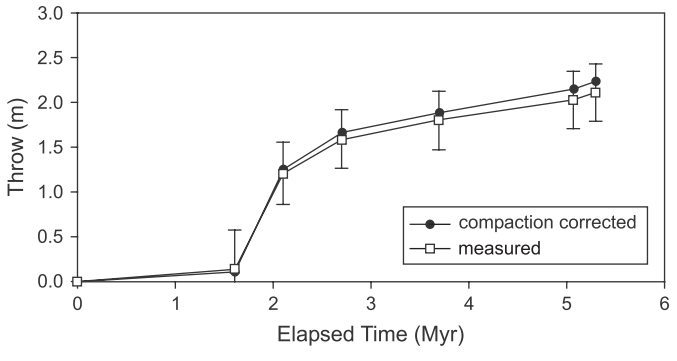

Fig. 9. Measured and compaction corrected displacement vs. Elapsed time (from deposition of the oldest horizon) curves for the Cape Egmont Fault. Both curves were derived by progressively backstripping fault displacements on depth converted interpretations of a seismic line close to the centre of the fault (line 86ma-38 from Nicol et al., 2005) (Fig. 8). The compaction correction was performed for a 40% sand and 60% shale sequence with initial porosities of 0.57–0.6 and coefficients of scaling (c) of 0.39–0.42.

Displacements track along the curves in Fig. 10 with the displacement loss being controlled by the difference in sediment compaction at the depth where displacement accrued on the fault surface (marked by the unfilled circles on the displacement loss curve) and the compaction at the final depth of burial (i.e. 5 km). For example, displacement that accrued on the fault at the surface loses about 50% of its original 10 m by the time it reaches 5 km depth, whilst displacement added to the fault surface at a depth of 3 km only decreases by 5% due to compaction.

Decreases in the percentage of displacement loss that accompany increases of growth index can also be attributed to the relative timing of faulting (i.e. displacement accumulation) and fault burial (Fig. 6). A high growth index (e.g. 10) requires that for a constant footwall depth, the depth of the same horizon in the hangingwall and the finite displacement would be greater than for a low growth index (e.g. 0.01). A footwall horizon depth of 1 km, for example, and a growth index of 10

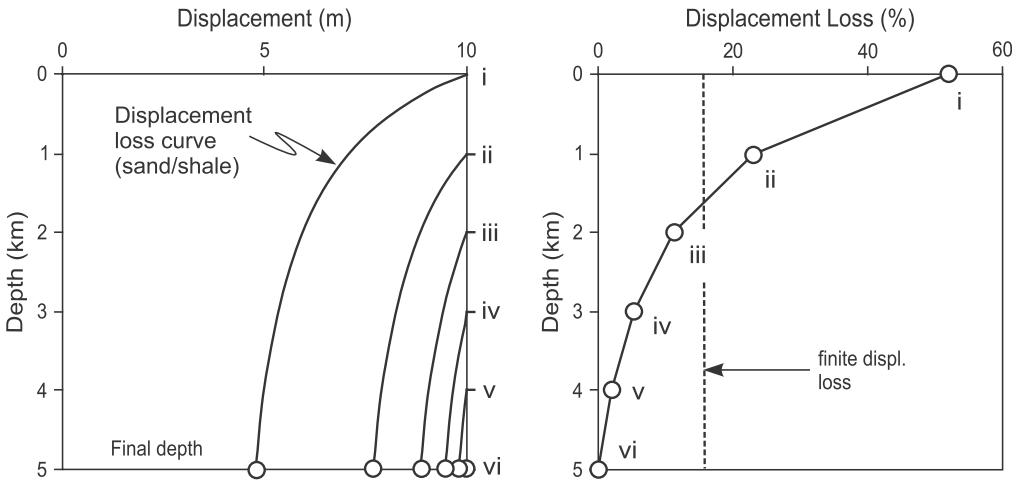

Fig. 10. Compaction-related displacement changes in a 50:50 sand/shale sequence for six increments of 10 m displacement which accrue on a progressively buried fault at depths of 0 km (i), 1 km (ii), 2 km (iii), 3 km (iv), 4 km (v) and 5 km (vi). (a) Displacement vs. depth curves showing how the preserved 10 m displacement for each increment (i–vi) decreases with depth. (b) Displacement loss (%) vs. depth of faulting, showing the percentage displacement losses for displacement increments accumulated at a particular depth of faulting and buried to 5 km depth. The percentage displacement loss of the entire 60 m displacement is about 15% (shown as broken line).

require a hangingwall horizon depth of 11 km and displacement of 10 km, whilst a growth index of 0.01 requires a depth of 1.01 km and a displacement of 10 m. In cases where growth indices are high, much of the displacement accrues at hangingwall depths of >3 km after much (c. 60–80%) of the sequence compaction has already taken place. The low proportional displacement losses for high growth indices are, therefore, a function of the relatively low compaction gradients at greater depths and the relatively high proportion of total displacement that accrues at these depths. The relatively low percentage losses of displacement for high growth indices are also a function of the high displacements necessary to produce the high growth indices. In a sand sequence, for example, the c. 2.8% displacement loss at a depth of 1 km and for a growth index of 10 requires about 280 m of displacement loss due to compaction, while a 0.01 growth index produces a 1 m displacement loss for a 10 m throw at 1 km depth in the same sequence (Fig. 6a). Therefore, in absolute terms displacement loss may increase for higher growth indices and thus require a greater amount of differential compaction across a fault, as would be expected.

The impact of the relative timing of faulting and sedimentation on compacted displacements is explored further in Fig. 7. Temporal changes in compacted and uncompacted displacements are charted for sand, shale and mixed (sand/shale) sequences with varying growth indices and for each of the three displacement histories in Fig. 2. The displacement history curves are backstripped displacement versus elapsed time plots in which the onset of sedimentation (and in Figs. 7a–c, g–i faulting) is at the origin and displacements accrue as deformation evolves (Fig. 7). For each plot the uncompacted displacement (thick black line) at the cessation of faulting is 500 m, with the constant displacement rates in Fig. 7d–i being twice those in Fig. 7a–c. The percentage displacement loss is independent of the fault displacement rates. The displacement history curves indicate that: (i) for the Constant and Early faulting models changes in displacement due to compaction vary with changes in growth indices, (ii) in the Late Faulting model lower growth indices (i.e. mainly 0.1 and 0.01) erroneously indicate some displacements prior to the onset of faulting, and (iii) the largest losses of displacement due to compaction for each lithology occur in the Early faulting model (Fig. 7).

The changing effects of compaction on displacement for different growth indices in Figs. 7a–c and g–i arise principally due to the exponential nature of compaction curves (Fig. 3) and the variable burial histories arising from the different growth indices. The variable burial histories occur because the fixed displacement rates for each of the three fault history models require variable sedimentation rates to achieve the range of growth indices. A growth index of 10 and displacement of 200 m would, for example, be associated with hangingwall and footwall sediment thicknesses of 220 and 20 m respectively, whilst a growth index of 0.1 would require thicknesses of 2200 and 2000 m for the same 200 m displacement. Therefore, the curves for each growth index differ because they occupy different parts of the compaction curves in Fig. 3 and, as a result, contain varying components of pre-compaction displacement. The smallest losses in displacement due to compaction occur for the lowest (0.01) and highest (10) growth indices. The small displacement losses for the low-growth index curves (0.01) occur because 90% of the displacement accrued on the fault at depths of 5 km or deeper and at these depths c. 80% or more of the compaction predates displacement accumulation (Fig. 3b). By contrast for a high growth index of 10, sediment and fault compaction in our models is restricted to depths of ≤550 m (because the maximum throw is 500 m) and, although sediments compact relatively quickly with increasing depth at these shallow levels, the limited depth range over which compaction takes place means that the total displacement loss is small in comparison to that for growth indices of 0.1 and 1 (Fig. 7).

In the Late Faulting model the low displacement rate ''tail'' present for lower growth indices incorrectly suggests that fault displacements initially accrued slowly before accelerating (Fig. 7d–f). In such cases using the backstripping method without accounting for compaction will provide estimated displacements for horizons immediately prior to the onset of faulting which are larger than the true values. The reason for these discrepancies is again the interplay between compaction and the timing of displacement accumulation. At lower growth indices the depth range over which displacements accrue on the faults is kilometres to tens of kilometres. Therefore, an increment of displacement, which for the models is constant along the cross-sectional length of a fault, will compact to a greater extent higher in the sequence than it does at depth. Thus, backstripping this displacement increment, i.e. by subtracting displacement close to the surface from all other displacements on older horizons, will not remove, or backstrip, the entire displacement increment from older horizons. As backstripping does not remove all displacement during a given growth increment some displacement remains when the faulting has been restored to the base of the growth sequence. The resulting erroneous ''pre-faulting'' displacements can be up to c. 10%, but is generally less than 5%, of the finite displacement (Fig. 7d–f) and would suggest that faulting began earlier than it did. These are, however, relatively small displacements, which will sometimes be on the scale of displacement measurement errors, and will also be even lower when the pre-faulting sequence is more compacted than the syn-faulting sequence (i.e. when the latter overlies ''basement'').

The large displacement losses in the Early Faulting model arise because faulting is followed by continued sedimentation and burial of the fault, which increases compaction and displacement loss. The amount of displacement loss associated with post-faulting burial is mainly dependent on the rock type, the degree of syn-faulting sequence compaction, and the amount of post-faulting burial. As with all other curves, displacement loss increases with shale content (Fig. 7g–i). Both the degree of syn-faulting compaction and the burial following faulting are determined in Fig. 7 by the growth index. A growth index of 10, for example, requires that both the maximum thickness of syn-faulting (550 m) and the post-faulting (50 m) sequences are small. Therefore, although the sequence is relatively uncompacted, the post-faulting compaction is small and, as a result, the displacement loss is minor (<4%). Similarly, displacement loss for a growth index of 0.01 are also low (<10%); however, in this case the low values arise because the displacements accrue on the fault after the surrounding sediments have undergone significant compaction and, as a consequence, post faulting compaction is small. In contrast, for a growth index of 0.1, 5 km of sediment blankets the fault and is associated with 20–30% total displacement loss (Fig. 7h). Approximately half of this displacement loss arises due to post-faulting compaction, however, burial of this fault by a further 5 km would only reduce displacement by a further 3% of the total precompaction 500 m. Therefore, circumstances in which post-faulting burial is large (e.g. >5 km) maximise the displacement loss due to compaction, particularly when the syn-fault sequence was at relatively shallow depths at the cessation of faulting. Even in these circumstances, however, the absolute losses of displacement may be >30% but the relative displacement losses of different horizons within the syn-faulting sequence will not be excessive and displacement backstripping will be capable of identifying the basic form of displacement curves.

4. Displacement changes; natural example results

To test the results of the modelling we compare compacted and uncompacted displacements for the Cape Egmont Fault, a large normal growth fault from the Taranaki Basin in New Zealand (Fig. 8). Analysis of the geometry of growth strata across the Cape Egmont Fault has previously provided a basis for establishing its displacement history on a broad range of time scales (Nicol et al., 2005; Manzocchi et al., 2006). Earlier work suggested that displacement losses arising from compaction would be less than 20% (Nicol et al., 2005), a relatively small error given the nature of previous work, and as a consequence decompaction of displacements was not performed. The modelling performed in this study provides a basis for testing the sensitivity of fault displacements to compaction. The Cape Egmont fault is characterised by a post-compaction growth index of <c. 10, within a mixed sand-shale sequence, with a maximum throw (vertical displacement) of c. 2 km on the section shown in Fig. 8b; displacements and growth indices decrease towards the lateral tips of the fault. The fault most closely matches the displacement history employed for generating Fig. 7e in which growth faulting is preceded by sediment deposition. In these conditions, our modelling suggests that displacement losses arising from compaction are low (i.e. c. 10%), a conclusion which supports the contention of previous work. Direct comparison of the natural and model data is, however, complicated by the larger displacements of the Cape Egmont fault (i.e. 2 km as opposed to 500 m in the models) and the variable, rather than constant, displacement rates. It is, however, possible to test the significance of compaction by comparing the results of displacement backstripping the Cape Egmont Fault, including and excluding compaction.

Displacement backstripping is performed by subtracting displacements on younger horizons from older horizons to define displacement distributions or displacement accumulation through time (Petersen et al., 1992; Childs et al., 1993). The method assumes that fault growth involves constant incremental displacements along the cross-sectional length of a fault (i.e. the same condition applied to our models). Backstripping of the Cape Egmont Fault show that to a first order the backstripped decompacted (calculated) and compacted (measured) displacements are the same (Fig. 9); the displacements are within the c. <±15% errors on displacement measurement (for further discussion see Nicol et al., 2005). The differences between compacted and decompacted displacements for the backstripped curves range from +16 m at 1.6 Myr through to −120 m at 5.3 Myr and are 6% and 12% of the measured displacements, respectively. These small differences between the compacted and decompacted displacements support previous

inferences suggesting that decompaction is not required to correctly interpret the first-order growth history of the fault (Nicol et al., 2005). Displacement data for this fault have previously been interpreted to define the onset of faulting to be at c. 3.7 Ma, which corresponds to an "elapsed time" of 1.7 Myr on Fig. 9 (Nicol et al., 2005; Manzocchi et al., 2006). Therefore, the very low displacements up to an elapsed time of 1.7 Myr were not taken to indicate fault movements over this time interval, a conclusion which is justified by the errors in displacement measurement, compounded by the errors associated with the calculation of incremental displacements. The latter is supported by the fact that the low displacements on Fig. 9 between 0 and 1.7 Myr elapsed time are reminiscent of our modelling results indicating that when compactable basinal sediments underlie the syn-faulting sequence (e.g. Fig. 7e), spurious indications of low pre-faulting displacements may be generated if compaction is not properly accounted for.

5. Discussion and conclusions

Results from numerical modelling of growth faults and a natural example compare well and together suggest that displacements in growth sequences typically decrease by no more than 20% (and is often much less) due to sediment compaction. The magnitude of these decreases is dependent on lithology, which controls the shape of the compaction curve, and the depth range over which fault displacements migrate along the compaction curves. In general, displacement loss due to compaction increases with increase in the percentage shale. The effect of burial depth on displacement loss is dependent on the relative amount of pre- and post-displacement compaction (Fig. 10). Determining the total displacement loss is complicated by the fact that cumulative displacement typically accumulates on a fault surface in many small (e.g. <5 m scale), sometimes co-seismic, increments, each characterised by lateral variations in displacements. Arising from this spatial variability, individual displacement increments at each location along a fault surface may be subjected to different compaction histories. These complications could be compounded by structural and stratigraphic effects which may be fault-independent but which are responsible for diverse pre and post incremental displacement compaction histories along the length of a fault (Fig. 10). In all cases, however, the decrease in displacement due to compaction is greatest for those incremental displacements which accrued on the fault near to the free surface (e.g. <0.5 km depth), where strata have relatively high porosities, and which are subsequently buried to significant depths (e.g. >5 km depth). Conversely, displacements of sedimentary rocks that have already experienced substantial burial (e.g. >5 km depth) and compaction, will preserve a greater proportion of the original displacement.

These two scenarios represent end-members in a continuum which, for growth sequences, principally arise due to variations in the relative rates of sedimentation and displacement (i.e. growth index). For syn-sedimentary normal faults imaged in seismic reflection lines, for example, growth indices are typically between 0.1 and 3 at depths of up to about 4 km and are therefore intermediate between the extremes modelled (see Childs et al., 2003). The displacement losses associated with faults with the range of growth indices typical of natural faults (i.e. 0.1–10) and for a broad range of displacements is shown in Fig. 6, and mainly vary between c. 5% and 15%. In these cases displacement loss due to compaction is relatively small and, for sand or mixed sand-shale sequences with growth indices of c. >0.1, decompaction is not required to decipher first-order uncompacted displacements and fault-growth histories. However, for sequences with high percentage shale (e.g. >70%) and low growth indices (e.g. <0.1), which may characterise deep marine environments with high sedimentation rates compared to displacement rates, consideration should be given to decompacting fault displacements. Even in these circumstances our modelling shows, however, that the likely displacement losses need not be as large as might have been expected and that the basic characteristics of fault growth can be gleaned from displacement backstripping without including decompaction. Decompaction may also be beneficial when post-faulting burial is several kilometres or more (e.g. Fig. 7g–i), and in circumstances where precise estimates of displacement, rather than general displacement trends, are required to refine fault-growth models. Nevertheless, in many circumstances decompaction will only significantly improve our constraints on fault growth when the porosity–depth curve and the relative timing of faulting and compaction of growth strata are well constrained, and where uncertainties on displacement measurements are small (e.g. <10%).

Acknowledgements

This paper is the result of studies completed with financial support from the Royal Society of New Zealand Marsden Fund (GNS 902), the Enterprise Ireland Basic Research Grant Scheme (SC/00/041) and the UCD President's Fellowship Scheme. We thank Eugenio Carminati and Eduard Kosa for their thorough and constructive reviews. We are also grateful to other members of the Fault Analysis Group for numerous technical discussions and we thank Mats Schöpfer for redrafting some of the figures.

Appendix

Sediment compaction equations associated with the models used in this paper are presented in this appendix. Porosity reduction with depth is typically modelled empirically from *in situ* measurements for a range of rock types and tectonic settings (e.g. Magara, 1976; Baldwin and Butler, 1985; Scherer, 1987; Stam et al., 1987; Schmoker and Gautier, 1988). The relationship between porosity and depth is defined by an exponential function, e.g. $\Phi(z) = \Phi_0 e^{-cz}$, where Φ_0 is the surface porosity, c is a scaling coefficient and z is the depth (e.g. Sclater and Christie, 1980; Korvin, 1984). In this paper we use the porosity–depth relationships of Sclater and Christie (1980) for sand, shale and mixed (sand/shale) sequences.

The relationship between porosity loss and volume loss (or thickness loss in the case of vertical confining pressure) with

depth can be defined if the volume of solid grains is assumed to be constant, the grains are taken to be incompressible and any dissolution and precipitation (chemical compaction) occurs on a local scale only. Porosity can be expressed as the fraction of the sediment that is made up of pore space, so that the length (i.e. thickness) of the solid fraction of this sediment is given by $(1-\Phi(z_0)) \times l_0$, where $\Phi(z_0)$ is the porosity of sediment at depth z_0 and l_0 is the length of the sediment package including pore space. If the sediment is buried deeper, to depth z_1, the porosity will decrease to $\Phi(z_1)$ and the sediment package will decrease in thickness (from l_0 to l_1), but the thickness of the solid fraction will remain the same such that

$$(1-\Phi_0)l_0 = (1-\Phi_1)l_1$$

and the change in length between the original length, l_0 and the compacted length l_1 is described by

$$\frac{l_1}{l_0} = \frac{(1-\Phi_0)}{(1-\Phi_1)}.$$

This calculation applies to thin sheets of sediment where the porosity is effectively the same at the top and the base. Fig. 3 shows the change in porosity with depth and the associated changes in sediment thickness and fault displacement with depth for sand (solid line), sandy-shale (dashed line) and shale (dotted line) using the values of Φ_0 and c given in Sclater and Christie (1980). As the porosity tends to zero at depth, a sediment column of unit thickness will tend toward a thickness of $1-\Phi_0$, where Φ_0 is the surface porosity. Most of the change in thickness occurs in the top 1–2 km of sediment (Fig. 3b).

In our models sediment layers have variable porosity from top to base, requiring modification to the above compaction calculations. These modified equations are solved using the methods described by Sclater and Christie (1980), where, for a column of sediment lying between depths z_1 and z_2, the thickness of the fluid fraction is equal to the integral of the porosity–depth function between z_1 and z_2, such that

$$l_w = \int_{z_1}^{z_2} \Phi_0 e^{-cz} dz$$

$$l_w = \frac{\Phi_0}{c}\left(e^{-cz_1} - e^{-cz_2}\right)$$

The thickness of the solid fraction of this sediment column is given by the total thickness, $z_2 - z_1$, minus the thickness of the fluid fraction;

$$l_{sf} = z_2 - z_1 - \frac{\Phi_0}{c}\left(e^{-cz_1} - e^{-cz_2}\right) \quad \text{(A1)}$$

If this sediment is moved to a new position, lying between z_1' and z_2', the porosity will change, but the thickness of the solid fraction will remain unchanged, and describes a new equation:

$$l_{sf} = z_2' - z_1' - \frac{\Phi_0}{c}\left(e^{-cz_1'} - e^{-cz_2'}\right) \quad \text{(A2)}$$

In our models z_1 and z_2 represent the positions of the footwall and hangingwall cutoffs following the imposition of an increment of displacement (i.e. Step 1 in text; Fig. 4). respectively, and z_1' represents the new position of the footwall after the subsidence step has been applied (i.e. Step 2). The new position of the hangingwall, taking into account the effects of sedimentary compaction (Step 3), z_2', can then be found by combining equations (A1) and (A2). The equation to be solved is;

$$z_2' - z_1' - z_2 + z_1 - \frac{\Phi_0}{c}\left(e^{-cz_1'} - e^{-cz_2'} - e^{-cz_1} + e^{-cz_2}\right) = 0$$

This equation cannot be solved directly, but must instead be solved iteratively using the Newton–Raphson method;

$$z_{new} = z - \frac{f(z)}{f'(z)}$$

$$z_{2new} = z_2 - \frac{z_2' + \frac{\Phi_0}{c}\left(e^{-cz_2'}\right) + z_1 - z_2 - z_1' + \frac{\Phi_0}{c}\left(e^{-cz_1} - e^{-cz_2} - e^{-cz_1'}\right)}{1 - \Phi_0 e^{-cz_2'}}$$

If the value of $z_{2\text{new}}$ does not provide a solution to the equation above then a new value of $z_{2\text{new}}$ is derived from the equation by replacing z_2' with the current value of $z_{2\text{new}}$. This process is repeated until a solution to the equation is found. The values of z_1' and z_2' become the new values of z_1 and z_2. The 3-step process is then repeated by first increasing z_2 by an amount equivalent to an increment of displacement. Because the porosity–depth function is integrated with respect to depth, the calculations are not influenced by the thickness of sediment added to the model at each step.

References

Baldwin, B., Butler, C.O., 1985. Compaction curves. American Association of Petroleum Geologists Bulletin 69, 622–626.

Barnett, J.A.M., Mortimer, J., Rippon, J.H., Walsh, J.J., Watterson, J., 1987. Displacement geometry in the volume containing a single normal fault. American Association of Petroleum Geologists Bulletin 71, 925–937.

Childs, C., Easton, S.J., Vendeville, B.C., Jackson, M.P.A., Lin, S.T., Walsh, J.J., Watterson, J., 1993. Kinematic analysis of faults in a physical model of growth faulting above a viscous salt analogue. Tectonophysics 228, 313–329.

Childs, C., Watterson, J., Walsh, J.J., 1995. Fault overlap zones within developing normal fault systems. Journal of the Geological Society, London 152, 535–549.

Childs, C., Nicol, A., Walsh, J.J., Watterson, J., 2003. The growth and propagation of synsedimentary faults. Journal of Structural Geology 25, 633–648.

Clausen, O.-R., Korstgard, J.A., Petersen, K., McCann, T., O'Reilly, B.M., Shannon, P.M., Howard, C.B., Mason, P.J., Walsh, J.J., Watterson, J., 1994. Systematics of faults and fault arrays. In: Helbig, K. (Ed.), Modeling the Earth for Oil ExplorationFinal Report of the CEC's Geoscience Program 1990–1993. Elsevier, pp. 205–316.

Davison, I., 1987. Normal fault geometry related to sediment compaction and burial. Journal of Structural Geology 9, 393–401.

Gibson, J.R., Walsh, J.J., Watterson, J., 1989. Modelling of bed contours and cross-sections adjacent to planar normal faults. Journal of Structural Geology 11, 317–328.

Hedberg, H.D., 1936. Gravitation compaction of clays and shales. American Journal of Science 231, 241–287.

Korvin, G., 1984. Shale compaction and statistical physics. Geophysical Journal Royal Astronomical Society 78, 35–50.

Lundegard, P.G., 1992. Sandstone porosity loss—a "big picture" view of the importance of compaction. Journal of Sedimentary Petrology 62, 250–260.

McLeod, A.E., Dawers, N.H., Underhill, J.R., 2000. The propagation and linkage of normal faults: insights from the Strathspey-Brent-Statfjord fault array, northern North Sea. Basin Research 12, 263–284.

Magara, K., 1976. Water expulsion from clastic sediments during compaction: directions and volume. American Association of Petroleum Geologists Bulletin 60, 543–553.

Manzocchi, T., Walsh, J.J., Nicol, A., 2006. Displacement accumulation from earthquakes on isolated normal faults. Journal of Structural Geology 28, 1685–1693.

Meyer, V., Nicol, A., Childs, C., Walsh, J.J., Watterson, J., 2002. Progressive localisation of strain during the evolution of a normal fault system in the Timor Sea. Journal of Structural Geology 24, 1215–1231.

Nicol, A., Walsh, J., Berryman, K., Nodder, S., 2005. Growth of a normal fault by the accumulation of slip over millions of years. Journal of Structural Geology 27, 327–342.

Perrier, R., Quiblier, J., 1974. Thickness changes in sedimentary layers during compaction history: methods for quantitative evaluation. American Association of Petroleum Geologists Bulletin 58, 507–520.

Petersen, K., Clausen, O.-R., Korstgård, J.A., 1992. Evolution of a salt-related listric growth fault near the D-1 well, block 5605, Danish North Sea: displacement history and salt kinematics. Journal of Structural Geology 14, 565–577.

Roux, W.F., 1979. The development of growth fault structures: AAPG Structural Geology School Course Notes, 33p.

Scherer, M., 1987. Parameters influencing porosity in sandstones: A model for sandstone porosity prediction. American Association of Petroleum Geologists Bulletin 71, 485–491.

Schlische, R.W., Young, S.S., Ackermann, R.V., Gupta, A., 1996. Geometry and scaling relations of a population of very small rift-related normal faults. Geology 24, 683–686.

Schmoker, J.W., Gautier, D.L., 1988. Sandstone porosity as a function of thermal maturity. Geology 16, 1007–1010.

Sclater, J.G., Christie, P.A.F., 1980. Continental stretching: an explanation of the post-mid-Cretaceous subsidence of the central North Sea Basin. Journal of Geophysical Research 85, 3711–3739.

Stam, B., Gradstein, F.M., Lloyd, P., Gillis, D., 1987. Algorithms for porosity and subsidence history 13, 317–349.

Walsh, J.J., Watterson, J., Yielding, G., 1991. The importance of small-scale faulting in regional extension. Nature 351, 391–393.

Walsh, J.J., Nicol, A., Childs, C., 2002. An alternative model for the growth of faults. Journal of Structural Geology 24, 1669–1675.

Watterson, J., 1986. Fault dimensions, displacements and growth. Pure and Applied Geophysics 124, 365–373.

Weller, J.M., 1959. Compaction of sediments. American Association of Petroleum Geologists Bulletin 43, 273–310.

Xiao, H.-B., Suppe, J., 1989. Role of compaction in listric shape of growth normal faults. American Association of Petroleum Geologists Bulletin 73, 777–786.